REFERENCES

[1] Willner, I.; and Katz, E. Bioelectronics - From Theory to Applications. Wiley-VCH, 1st ed. 2005

[2] Siebert, F.; and Hildebrandt, P. Vibrational Spectroscopy in Life Sciences. Wiley-VCH, 1st ed. 2008.

[3] Murgida, D. H.; and Hildebrandt, P. Redox and Redox-Coupled Processes of Heme Proteins and Enzymes at Electrochemical Interfaces. Phys. Chem. Chem. Phys. 7 (2005): 3773-3784.

[4] Murgida, D. H.; and Hildebrandt, P. Disentangling Interfacial Redox Processes of Proteins by SERR Spectroscopy. Chem. Soc. Rev. 37 (2008): 937-945.

[5] Smulevich, G.; and Spiro, T. G. Surface Enhanced Raman Spectroscopic Evidence that Adsorption on Silver Particles Can Denature Heme Proteins. J. Phys. Chem. 89 (1985): 5168-5173.

[6] Ataka, K.; and Heberle, J. Functional Vibrational Spectroscopy of a Cytochrome c Monolayer: SEIDAS Probes the Interaction with Different Surface-Modified Electrodes. J. Am. Chem. Soc. 126 (2004): 9445-9457.

[7] Ataka, K.; Giess, F.; Knoll, W.; Naumann, R.; Haber-Pohlmeier, S.; Richter, B.; and Heberle, J. Oriented Attachment and Membrane Reconstitution of His-Tagged Cytochrome c Oxidase to a Gold Electrode: In Situ Monitoring by Surface-Enhanced Infrared Absorption Spectroscopy. J. Am. Chem. Soc. 126 (2004): 16199-16206.

[8] Ataka, K.; and Heberle, J. Biochemical Applications of Surface-Enhanced Infrared Absorption Spectroscopy. Anal. Bioanal. Chem. 388 (2007): 47-54.

[9] Murphy, R. E.; and Sakai, H. Aspen International Conference On Fourier Spectroscopy. G. A. Vanasse, A. T. Stair, and D.J. Baker, eds. 1970.

[10] Murphy, R. E., Cook, F. M., and Sakai, H. Time-resolved Fourier

Spectroscopy. J. Opt. Soc. Am. 65 (1975): 600-604.

[11] Mantz, A. W. Infrared Multiplexed Studies of Transient Species. Appl. Spectrosc. 30 (1976): 459-461.

[12] Mantz, A. W. Infrared Spectroscopic Studies of Transients. Appl. Opt. 17 (1978): 1347-1351.

[13] Griffiths, P. R.; and de Haseth, J. A. Fourier Transform Infrared Spectroscopy. John Wiley & Sons, New York, 1986.

[14] Diem, M. Modern Vibrational Spectroscopy. J. Wiley & Sons, New York, 1993.

[15] Osawa, M.; Yoshii, K.; Ataka, K; and Yotsuyanagi, T. Real-Time Monitoring of Electrochemical Dynamics by Submillisecond Time-Resolved Surface-Enhanced Infrared Attenuated-Total-Reflection Spectroscopy. Langmuir 10 (1994): 640-642.

[16] Johnson, T. J.; and Zachmann, G. Introduction to Step-Scan FTIR. Bruker.

[17] Goormaghtigh, E.; Raussens, V.; Ruysschaert, J. M. Attenuated Total Reflection Infrared Spectroscopy of Proteins and Lipids in Biological Membranes. Biochim. Biophys. Acta. 1422 (1999): 105-185.

[18] Rich, P. R.; and Breton, J. Attenuated Total Reflection Fourier Transform Infrared Studies of Redox Changes in Bovine Cytochrome c Oxidase: Resolution of the Redox Fourier Transform Infrared Difference Spectrum of Heme a3. Biochemistry 41 (2002): 967-973.

[19] Vigano, C.; Manciu, L.; Buyse, F.; Goormaghtigh, E.; Ruysschaert, J. M. Attenuated Total Reflection IR Spectroscopy as a Tool to Investigate the Structure, Orientation and Tertiary Structure Changes in Peptides and Membrane Proteins. Biopolymers 55 (2000): 373–380.

[20] Saux, L. A.; Ruysschaert, J. M.; and Goormaghtigh, E. Membrane Molecule Reorientation in an Electric Field Recorded by Attenuated Total Reflection Fourier-Transform Infrared Spectroscopy. Biophys. J. 80 (2001): 324–330.

[21] Hartstein, A.; Kirley, J. R.; and Tsang, J. C. Enhancement of the Infrared

Absorption from Molecular Monolayers with Thin Metal Overlayers. Phys. Rev. Lett. 45 (1980): 201-204.

[22] Osawa, M. Handbook of Vibrational Spectroscopy. Chalmers, J. M., Griffiths, P. R., Eds. Vol. 1. John Wiley & Sons, New York, 2002.

[23] Miyake, H.; Ye, S.; and Osawa, M. Electroless Deposition of Gold Thin Films on Silicon for Surface-Enhanced Infrared Spectroelectrochemistry. Electrochem. Comm. 4 (2002): 973-977.

[24] Singh, B. R. Infrared Analysis of Peptides and Proteins: Principles and Applications. American Chemical Society, ACS Symposium Series, 2000.

[25] Bushnell, G. W.; Louie, G. V.; and Brayer, G. D. High-Resolution Three-Dimensional Structure of Horse Heart Cytochrome c. J. Mol. Biol. 214 (1990): 585-595.

[26] Murgida, D. H.; and Hildebrandt, P. Heterogeneous Electron Transfer of Cytochrome c on Coated Silver Electrodes: Electric Field Effects on Structure and Redox Potential. J. Phys. Chem. B 105 (2001): 1578-1586.

[27] Oellerich, S.; Wackerbarth, H.; and Hildebrandt, P. Spectroscopic Characterization of non-Native Conformational States of Cytochrome C. J. Phys. Chem. B 106 (2002): 6566-6580.

[28] Oellerich, S.; Lecomte, S.; Paternostre, M.; Heimburg, T.; and Hildebrandt, P. Peripheral and Integral Binding of Cytochrome *c* to Phospholipids Vesicles. J. Phys. Chem. B 108 (2004): 3871-3878.

[29] Murgida, D. H.; and Hildebrandt, P. Electron-Transfer Processes of Cytochrome *c* at Interfaces. New Insights by Surface-Enhanced Resonance Raman Spectroscopy. Acc. Chem. Res. 37 (2004): 854-861.

[30] Wackerbarth, H.; and Hildebrandt, P. Redox and Conformational Equilibria and Dynamics of Cytochrome c at High Electric Fields. Chemphyschem 4 (2003): 714-724.

[31] Murgida, D. H.; and Hildebrandt, P. Electrostatic-Field Dependent Activation Energies Modulate Electron Transfer of Cytochrome c. J. Phys. Chem. B 106 (2002): 12814-12819.

[32] Moss, D.; Nabedryk, E.; Breton, J.; and Maetele, W. Redox-Linked Conformational Changes in Proteins Detected by a Combination of IR Spectroscopy and Protein Electrochemistry. Eur. J. Biochem. 187 (1990): 565-572.

[33] Eddowes, M. J.; and Hill, H. A. O. Electrochemistry of Horse Heart Cytochrome c. J. Am. Chem. Soc. 102 (1979): 4461-4464.

[34] Avila, A.; Gregory, B. W.; Niki, K.; and Cotton, T. M. An Electrochemical Approach to Investigate Gate Electron Transfer using a Physiological Model System: Cytochrome c Immobilized on Carboxylic Acid-Terminated Alkanethiol SAMs on Gold Electrodes. J. Phys. Chem. B 104 (2000): 2759-2766.

[35] Ulman, A. Formation and Structure of Self-Assembled Monolayers. Chem. Rev. 96 (1996): 1533-1554.

[36] Ito, E.; Konno, K.; Noh, J.; Kanai, K.; Ouchi, Y.; Seki, K.; and Hara, M. Chain Length Dependence of Adsorption Structure of COOH-Terminated Alkanethiol SAMs on Au(111). Appl. Surf. Sci. 244 (2005): 584–587.

[37] Dannenberger, O.; Buck, M.; and Grunze, M. Self-Assembly of n-Alkanethiols: A Kinetic Study by Second Harmonic Generation. J. Phys. Chem. B 103 (1999): 2202–2213.

[38] Dai, Z.; and Ju, H. Effect of Chain Length on the Surface Properties of an ω-Carboxylalkanethiol Self-Assembled Monolayers. Phys. Chem. Chem. Phys. 3 (2001): 3769-3773.

[39] Chung, C.; and Lee, M. Self-Assembled Monolayers of Mercaptoacetic Acid on Ag Powder: Characterization by FT-IR Diffuse Reflection Spectroscopy. Bull. Korean. Chem. Soc. 25 (2004): 1461-1462.

[40] Smith, C. P.; and White, H. S. Theory of the Interfacial Potential Distribution and Reversible Voltammetric Response of Electrodes Coated with Electroactive Molecular Films. Anal. Chem. 64 (1992): 2398-2405.

[41] Lecomte, S.; Hildebrandt, P.; and Soulimane, T. Dynamics of the Heterogeneous Electron-Transfer Reaction of Cytochrome c (552) from Thermus Thermophilus. A Time-Resolved Surface-Enhanced

Resonance Raman Spectroscopic Study. J. Phys. Chem. B 103 (1999): 10053-10064.

[42] Clarke, R. J. The Dipole Potential of Phospholipid Membranes and Methods for its Detection. Adv. Coll. Int. Sci. 89 (2001): 263-281.

[43] Oklejas, V.; Sjostrom, C.; Harris, J. M.; and Disci-pline: Chemistry, Physical. Surface-Enhanced Raman Scattering Based Vibrational Stark Effect as a Spatial Probe of Interfacial Electric Fields in the Diffuse Double Layer. J. Phys. Chem. B 107 (2003), 7788-7794.

[44] Oklejas, V.; and Harris, J. M. In-Situ Investigation of Binarycomponent Self-Assembled Monolayers: A SERS-Based Spectroelectrochemical Study of the Effects of Monolayer Composition on Interfacial Structure. Langmuir 19 (2003), 5794-5801.

[45] Lorenz, L. Schwingungsspektroskopische Untersuchung von selbstorganisierten Monoschichten aus bifunktionellen Thiolen. Master's thesis, TU Berlin, (2004).

[46] Marcus, R. A. Theory of Oxidation-Reduction Reactions Involving Electron Transfer .1. J. Chem. Phys. 5, 24(1956): 966-978.

[47] Marcus, R. A.; and Sutin, N. Electron Transfers in Chemistry and Biology. Biochim. Biophys. Acta. 811 (1985): 265-322.

[48] Bolton, J. R.; Mataga, N.; and Mclendon, G. Introduction to Electron-Transfer in Inorganic, Organic, and Biological-Systems. Adv. Chem. Series 228 (1991): 1-6.

[49] Marcus, R. A. Electron Transfer Reactions in Chemistry - Theory and Experiment. J. Electroanal. Chem. 438 (1997): 251-259.

[50] Miller, J. R.; Beitz, J. V.; and Huddleston, R. K. Effect of Free-Energy on Rates of Electron-Transfer Between Molecules. J. Am. Chem. Soc. 106 (1984): 5057-5068.

[51] Closs, G. L.; Calcaterra, L. T.; Green, N. J.; Penfield, K. W.; and Miller, J. R. Distance, Stereoelectronic Effects, and the Marcus Inverted Region in Intramolecular Electron-Transfer in Organic Radical-Anions. J. Phys. Chem. 90 (1986), 3673-3683.

[52] Jortner, J. Temperature-Dependent Activation-Energy for Electron-Transfer

Between Biological Molecules. J. Chem. Phys. 64 (1976): 4860-4867.

[53] Kestner, N. R.; Logan, J.; and Jortner, J. Thermal Electron-Transfer Reactions in Polar-Solvents. J. Phys. Chem. 78 (1974): 2148-2166.

[54] Ulstrup, J.; and Jortner, J. Effect of Intramolecular Quantum Modes on Free-Energy Relationships for Electron-Transfer Reactions. J. Chem. Phys. 63 (1975): 4358-4368.

[55] Levich, V. G. and Dogonadze, R. R. Theory of Non-Radiation Electron Transitions from Ion to Ion in Solutions. Doklady Akademii Nauk Sssr 124 (1959): 123-126.

[56] Gosavi, S.; and Marcus, R. A. Nonadiabatic Electron-Transfer at Metal Surfaces. J. Phys. Chem. B 104 (2000): 2067-2072.

[57] Chidsey, C. E. D. Free-Energy and Temperature-Dependence of Electron-Transfer at the Metal-Electrolyte Interface. Science 251(1991): 919-922.

[58] Nahir, T. M. and Bowden, E. F. The Distribution of Standard Rate Constants for Electron Transfer between Thiol-Modified Gold Electrodes and Adsorbed Cytochrome c. J. Electroanal. Chem. 410 (1996): 9-13.

[59] Nahir, T. M.; Clark, R. A.; and Bowden, E. F. Linear-Sweep Voltammetry of Irreversible Electron-Transfer in Surface-Confined Species Using the Marcus Theory. Anal. Chem. 66 (1994): 2595-2598.

[60] Murgida, D. H.; and Hildebrandt, P. Proton-Coupled Electron Transfer of Cytochrome c. J. Am. Chem. Soc. 123 (2001): 4062-4068.

[61] Zhou, J.; Zheng, J.; and Jiang, S. Molecular Simulation Studies of the Orientation and Conformation of Cytochrome c Adsorbed on Self-Assembled Monolayers. J. Phys. Chem. B 108 (2004): 17418-17424.

[62] Duevel, R. V.; and Corn, R. M. Amide and Ester Surface Attachment Reactions for Alkanethiol Monolayers at Gold Surfaces As Studied by Polarization Modulation Fourier Transform Infrared Spectroscopy. Anal. Chem. 64 (1992): 337-342.

[63] Nagaoka, H.; and Imae, T. Poly(Amino Amine) Dendrimer Adsorption onto

3-Mercaptopropionic Acid SAM Formed on Au Surface-Investigation by Surface Enhanced Spectroscopy and Surface Plasmon Sensing. Transactions of Materials Research Society of Japan 26 (2001): 945-948.

[64] Me'thivier, C.; Beccard, B.; and Pradier, C. M. In Situ Analysis of a Mercaptoundecanoic Acid Layer on Gold in Liquid Phase by PM-IRAS. Evidence for Chemical Changes with the Solvent. Langmuir 19 (2003): 8807-8812.

[65] Jordan, C. E.; Frey, B. L.; Kornguth, S.; and Corn, R. M. Characterization of Poly-L-Lysine Adsorption onto Alkanethiol-Modified Gold Surfaces with Polarization-Modulation FTIR Spectroscopy and Surface Plasmon Resonance Measurements. Langmuir 10 (1994): 3642-3648.

[66] Imae, T.; and Torii, H. In Situ Investigation of Molecular Adsorption on Au Surface by Surface-Enhanced Infrared Absorption Spectroscopy. J. Phys. Chem. B 104 (2000): 9218-9224.

[67] Calvert, J. F.; Hill, J. L.; and Dong, A. Redox-Dependent Conformational Changes are Common Structural Features of Cytochrome c from Various Species. Arc. Biochem. Biophys. 346 (1997): 287–293.

[68] Dong, A.; Huang, P.; and Caughey, W. S. Redox-Dependent Changes in β-Extended Chain and Turn Structures of Cytochrome c in Water Solution Determined by Second Derivative Amide I Infrared Spectra. Biochemistry 31 (1992): 182-189.

[69] Dong, A.; Huang, P.; and Caughey, W. S. Protein Secondary Structures in Water from Second-Derivative Amide I Infrared Spectra. Biochemistry 29 (1990): 3303-3308.

[70] Feng, Y.; Roder, H.; and Englander, S. W. Redox-Dependent Structure Change and Hyperfine Nuclear Magnetic Resonance Shifts in Cytochrome c. Biochemistry 29 (1990): 3494-3504.

[71] Qi, P. X.; Stefano, D. L. D.; and Wand, A. J. Solution Structure of Horse Heart Ferrocytochrome c Determined by High-Resolution NMR and Restrained Simulated Annealing. Biochemistry 33 (1994): 6408-6417.

[72] Lo, T.; Guillemette, J. G.; Louie, G. V.; Smith, M.; and Brayer, G. D. Structural Studies of the Roles of Residues 82 and 85 at the Interactive Face of Cytochrome c. Biochemistry 34 (1995): 163-171.

[73] Takano, T.; and Dickerson, R. E. Conformation Change of Cytochrome *c*: I. Ferrocytochrome *c* Structure Refined at 1·5 Å Resolution. J. Mol. Biol. 153 (1981): 79-94.

[74] Schlereth, D. D.; and Maentele, W. Electrochemically Induced Conformational Changes in Cytochrome c Monitored by FTIR Difference Spectroscopy: Influence of Temperature, pH, and Electrode Surfaces. Biochemistry 32 (1993): 1118-1126.

[75] Schlereth, D. D.; and Mantele, W. Redox-Induced Conformational Changes in Myoglobin and Hemoglobin: Electrochemistry and Ultraviolet-Visible and Fourier Transform Infrared Difference Spectroscopy at Surface-modified Gold Electrodes in an Ultra-Thin-Layer Spectroelectrochemical Cell. Biochemistry 31 (1992): 7494-7502.

[76] Susi, H.; and Byler, D. M. Protein Structure by Fourier Transform Infrared Spectroscopy: Second Derivative Spectra. Biochem. Biophys. Res. Comm. 115 (1983): 391-397.

[77] Berghuis, A. M.; and Brayer, G. D. Oxidation State-Dependent Conformational Changes in Cytochrome C J. Mol. Biol. 223 (1992): 959-976.

[78] Edmiston, P. L.; Lee, J. E.; Cheng, S. S.; Saavedra, S. S. Molecular Orientation Distributions in Protein Films. 1. Cytochrome *c* Adsorbed to Substrates of Variable Surface Chemistry. J. Am. Chem. Soc. 119 (1997): 560-570.

[79] Macdonald, I. D. G.; Smith, W. E. Orientation of Cytochrome *c* Adsorbed on a Citrate-Reduced Silver Colloid Surface. Langmuir 12 (1996): 706-713.

[80] Walker, D. S.; Hellinga, H. W.; Saavedra, S. S.; Reichert, W. M. Integrated Optical Waveguide Attenuated Total Reflection Spectrometry and Resonance Raman Spectroscopy of Adsorbed Cytochrome c. J. Phys. Chem. 97 (1993): 10217-10222.

[81] Song, S.; Clark, R. A.; Bowden, E. F.; and Tarlov, M. J. Characterization of Cytochrome c/Alkanethiolate Structures Prepared by Self-Assembly on Gold. J. Phys. Chem. 97 (1993): 6564-6572.

[82] Clark, R. A.; and Bowden, E. F. Voltammetric Peak Broadening for Cytochrome *c*/Alkanethiolate Monolayer Structures: Dispersion of Formal Potentials. Langmuir 13 (1997): 559-565.

[83] Hamelin, A. Coadsorption of Sulphate Ions and Pyridine on the (111), (110) and (100) Faces of Gold. J. Electroanal. Chem. 144 (1983): 365-372.

[84] Valette, G.; and Hamelin, A. Structure et Propriétés de la Couche Double électrochimique à l'interphase Argent/Solutions Aqueuses de Fluorure de Sodium. J. Electroanal. Chem. 45 (1973): 301-319.

[85] Shlepakov, A. V.; and Sevastyanov, E. S. Sov. Electrochem. 14 (1978): 243.

[86] Ramirez, P.; Andreu, R.; Cuesta, A.; Calzado, C. J.; and Calvente, J. J. Determination of the Potential of Zero Charge of Au(111) Modified with Thiol Monolayers. Analytical Chemistry 79 (2007): 6473.

[87] Heimburg, T.; Marsh, D. Investigation of Secondary and Tertiary Structural Changes of Cytochrome c in Complexes with Anionic Lipids using Amide Hydrogen Exchange Measurements: an FTIR Study. Biophys. J. 65 (1993): 2408-2417.

[88] Kranich, A.; Hildebrandt, P.; Ly, K.; and Murgida, D. H. Direct Observation of the Gating Step in Protein Electron Transfer: Electric-Field-Controlled Protein Dynamics. J. Am. Chem. Soc. 30, 130 (2008): 9844–9848.

[89] Feng, Z. Q.; Imabayashi, S.; Kakiuchi, T.; and Niki, K. Long-Range Electron-Transfer Reaction Rates to Cytochrome c Across Long- and Short-Chain Alkanethiol Self-Assembled Monolayers: Electroreflectance Studies. J. Chem. Soc., Faraday Trans. 93 (1997): 1367-1370.

[90] Groot, M. T.; Merkx, M.; and Koper, M. T. M. Reorganization of Immobilized Horse and Yeast Cytochrome *c* Induced by pH

Changes or Nitric Oxide Binding. Langmuir 23 (2007): 3832-3839.

[91] Yue, H. J.; Khoshtariya, D.; Waldeck, D. H.; Grochol, J.; Hildebrandt, P.; and Murgida, D. H. On the Electron Transfer Mechanism Between Cytochrome *c* and Metal Electrodes. Evidence for Dynamic Control at Short Distances. J. Phys. Chem. B 110 (2006): 19906-19913.

[92] Wei, J. J.; Liu, H. Y.; Dick, A. R.; Yamamoto, H.; He, Y. F.; and Waldeck, D. H. Direct Wiring of Cytochrome *c*'s Heme Unit to an Electrode: Electrochemical Studies. J. Am. Chem. Soc. 124 (2002): 9591-9599.

[93] Dolidze, T. D.; Rondinini, S.; Verto-Va, A.; Waldeck, D. H.; and Khoshtariya, D. E. Impact of Self-Assembly Composition on the Alternate Interfacial Electron Transfer for Electrostatically Immobilized Cytochrome *C*. Biopolymers 87 (2007): 68-73.

[94] Leopold, M. C.; Black, J. A.; and Bowden, E. F. Influence of Gold Topography on Carboxylic Acid Terminated Self-Assembled Monolayers. Langmuir 18 (2002): 978-980.

[95] Laviron, E. General Expression of the Linear Potential Sweep Voltammogram in the case of Diffusionless Electrochemical Systems. J. Electroanal. Chem. 101 (1979): 19-28.

[96] Walczak, M. M.; Chung, C. K.; Stole, S. M.; Widrig, C. A.; and Porter, M. D. Structure and interfacial properties of spontaneously adsorbed n-alkanethiolate monolayers on evaporated silver surfaces. J. Am. Chem. Soc. 113 (1991): 2370-2378.

[97] Love, J. C.; Estroff, L. A.; Kriebel, J. K.; Nuzzo, R. G.; and Whitesides, G. M. Self-Assembled Monolayers of Thiolates on Metals as a Form of Nanotechnology. Chem. Rev. 105 (2005): 1103-1169.

[98] Laibinis, P. E.; Whitesides, G. M.; Allara, D. L.; Tao, Y. T.; Parikh, A. N.; and Nuzzo, R. G. Comparison of the Structures and Wetting Properties of Self-Assembled Monolayers of n-Alkanethiols on the Coinage Metal Surfaces, Copper, Silver, and Gold. J. Am. Chem. Soc. 113 (1991): 7152-7167.

[99] Bain, C. D.; Troughton, E. B.; Tao, Y. T.; Evall, J.; Whitesides, G. M.; and

Nuzzo, R. G. Formation of Monolayer Films by the Spontaneous Assembly of Organic Thiols from Solution onto Gold. J. Am. Chem. Soc. 111 (1989): 321-335.

APPENDIX

Redox-Linked Protein Dynamics of Cytochrome c

Probed by Time-Resolved Surface Enhanced Infrared Absorption Spectroscopy

Nattawadee Wisitruangsakul, Ingo Zebger, Khoa H. Ly, Daniel H. Murgida,

Sanong Ekgasit, and Peter Hildebrandt

Physical Chemistry Chemical Physics 10 (2008): 5276–5286.

PAPER www.rsc.org/pccp | Physical Chemistry Chemical Physics

Redox-linked protein dynamics of cytochrome c probed by time-resolved surface enhanced infrared absorption spectroscopy†

Nattawadee Wisitruangsakul,[ac] Ingo Zebger,*[a] Khoa H. Ly,[a] Daniel H. Murgida,[b] Sanong Ekgasit[c] and Peter Hildebrandt*[a]

Received 17th April 2008, Accepted 29th May 2008
First published as an Advance Article on the web 27th June 2008
DOI: 10.1039/b806528d

Time-resolved surface enhanced infrared absorption (SEIRA) spectroscopy is employed to analyse the dynamics of the protein structural changes coupled to the electron transfer process of immobilised cytochrome c (Cyt-c). Upon electrostatic binding of Cyt-c to Au electrodes coated with self-assembled monolayers (SAMs) of carboxyl-terminated thiols, cyclic voltammetric measurements demonstrate a reversible redox process with a redox potential that is similar to that of Cyt-c in solution, and a non-exponential distance-dependence of the electron transfer rate as observed previously (D. H. Murgida and P. Hildebrandt, *Chem. Soc. Rev.* 2008, 37, 937). On the basis of characteristic redox-state-sensitive amide I bands, the protein structural changes triggered by the electron transfer are monitored by rapid scan and step scan SEIRA spectroscopy in combination with the potential jump technique. Whereas the temporal evolution of the conjugate bands at 1693 and 1673 cm^{-1} displays the same rate constants as electron transfer, the time-dependent changes of the 1660-cm^{-1} band are slower by about a factor of 2. The study demonstrates that time-resolved SEIRA spectroscopy provides further information about the dynamics and mechanism of interfacial processes of redox proteins, thereby complementing the results obtained from other surface-sensitive techniques. In comparison with previous surface enhanced resonance Raman spectroscopic findings, the present results are discussed in terms of the local electric field strengths at the Au/SAM/Cyt-c interface.

Introduction

Immobilisation of redox enzymes on electronic conducting materials is a key issue in the design and construction of bioelectronic devices that are of actual or potential importance for biotechnological applications.[1] These hybrid systems aim to utilise the evolutionarily optimised electron transfer properties as well as substrate and product specificity of biocatalysts. The central challenge, however, is to achieve an efficient electronic coupling of the protein to inorganic materials, which is essential for the performance of bioelectronic devices. The enormous research efforts in this field follow empirical "trial-and-error" approaches or rational design principles to optimize the desired functional properties of the bioelectronic hybrid system. The latter strategy requires deeper insight into the molecular processes of immobilised proteins and the factors that control the electronic coupling with the conducting support. Progress in this respect strongly depends on appropriate techniques that may provide information about the structure and reaction dynamics of immobilised proteins.

Surface enhanced vibrational spectroscopies fulfil these requirements.[2] Among them surface enhanced resonance Raman (SERR) spectroscopy can be considered as an established technique for probing the molecular structure of the redox site and its dynamics and reactivity in interfacial processes.[3,4] For many systems, specifically for heme proteins, a drawback of this technique is the restriction to Ag surfaces since this metal limits the accessible electrode potential range. Moreover, Ag cations are known to attack proteins and thus may cause their denaturation.[5] Finally, SERR spectroscopy only probes the redox site but does not provide direct information about the protein structure and dynamics. In this respect, surface enhanced infrared absorption (SEIRA) spectroscopy represents a promising complementary method as demonstrated by the pioneering work of Ataka and Heberle.[6–8] The authors have successfully employed SEIRA spectroscopy to probe soluble and membrane bound proteins immobilised on coated Au electrodes. In general, the technique is used in the difference mode and thus reveals potential-dependent changes of the protein structure and its orientation. Specifically, it allows analysing redox transitions of heme proteins and enzymes.

In this work, we report for the first time the combination of SEIRA spectroscopy with time-resolved methods to monitor the electron transfer kinetics and protein dynamics of

[a] *Technische Universität Berlin, Institut für Chemie, Sekr. PC 14, Straße des 17. Juni 135, D-10623 Berlin, Germany. E-mail: hildebrandt@chem.tu-berlin.de, ingo.zebger@tu-berlin.de*
[b] *Departamento de Química Inorgánica, Analítica y Química Física/ INQUIMAE-CONICET, Facultad de Ciencias Exactas y Naturales, Universidad de Buenos Aires. Ciudad Universitaria, Pab. 2, piso 1, Buenos Aires, C1428EHA, Argentina*
[c] *Sensor Research Unit, Department of Chemistry, Faculty of Science, Chulalongkorn University, Phayathai Road, Patumwan, Bangkok, 10330, Thailand*

† Electronic supplementary information (ESI) available: Description of the model for approximating the electric field strength and the protein/SAM interface. See DOI: 10.1039/b806528d

immobilised cytochrome c (Cyt-c). The approach is based on the rapid-scan and step-scan methods that are well established in conventional Fourier-transform IR spectroscopy.[2] Similar to time-resolved SERR spectroscopy,[2,3] the processes to be studied are initiated by a rapid potential jump at the working electrode such that the subsequent relaxation processes can be probed by SEIRA spectroscopy, operated in the rapid scan and step scan mode for processes slower and faster than 100 ms. The present results demonstrate that SEIRA spectroscopy in conjunction with SERR spectroscopy and electrochemical methods may provide novel insight into the mechanism and dynamics of interfacial processes of proteins.

Materials and methods

Materials

6-Mercaptohexanoic acid (C5) from Dojindo and 16-mercaptohexadecanoic acid (C15) and 11-mercaptoundecanoic acid (C10), both purchased from Sigma-Aldrich, were used without further purification. Horse heart cytochrome c (Cyt) from Sigma-Aldrich was purified by HPLC. The water used in all experiments was purified by a Millipore system and its resistance was more than 18 MΩ. All other chemicals were of highest purity grade available.

SEIRA measurements

SEIRA measurements were performed with a Kretschmann-ATR configuration using a semi-cylindrical shaped silicone (Si) crystal (20 × 25 × 10 mm of W × L × H) under an angle of incidence of 60°. Thin gold (Au) films were formed on the flat surface of the Si substrate by an electroless (chemical) deposition technique.[9] The formation of SAMs followed the protocol described previously.[10,11] For Cyt-c adsorption SAM-coated electrodes were immersed in Cyt-c solution using a concentration of 2 μM. The SEIRA spectra were recorded from 4000 to 1000 cm^{-1} with a spectral resolution of 4 cm^{-1} on a Bruker IFS66v/s spectrometer equipped with a photoconductive MCT detector. 400 scans were co-added for a spectrum.

For the spectro-electrochemical measurements the ATR crystal was incorporated into a three-electrode home-built cell that was constructed on the basis of a previously published design.[8] The Au-film on the ATR crystal (0.9 cm^2 geometric area, 2.52 cm^2 real area after correction with a roughness factor of 2.8), a Pt wire, and a Ag/AgCl (3 M KCl) electrode served as working, counter, and reference electrode, respectively. The total filling volume of the cell was 6 mL. Electrode potentials were controlled by an Autolab PGSTAT 12 potentiostat under control of the related GPES software. All potentials cited in this work refer to the Ag/AgCl electrode.

Redox-induced SEIRA difference spectra of Cyt-c were measured using a single-beam spectrum, recorded at −0.1 V, as a reference, where the adsorbed Cyt-c is fully reduced. Sample spectra were measured at different electrode potentials (−0.08, −0.06, −0.04, −0.02, 0.00, 0.02, 0.04, 0.06, 0.08, 0.10, 0.125 and 0.15 V) using a newly measured background spectrum in each case. All spectra were measured after equilibration of the system at the respective electrode potential for 60 s. During the measurements which were carried out at ambient temperature (26 °C), the solution was purged with Ar. All experiments were carried out at pH 7.0 with 10 or 30 mM phosphate buffer corresponding to an ionic strength (I) of *ca.* 22 mM and 66 mM, respectively.

Redox-induced IR difference spectra of Cyt-c in solution were measured with a spectroelectrochemical cell, at 5 °C in 50 mM phosphate buffer (pH 7), with 100 mM NaCl and a cocktail of redox mediators, covering the potential range under investigation, as described previously.[12]

Time-resolved SEIRA measurements

Time-resolved (TR) SEIRA experiments were carried out in the same SEIRA electro-chemical setup described above using the potential jump technique.[2] Spectra acquisition was synchronized with the potential jumps controlled by a home-made pulse delay generator. Series of time dependent single-channel spectra of Cyt-c were collected when a potential jump was carried out from the reference potential (Cyt-c largely reduced) to the redox potential, and for the reverse jump. Depending on the time scale under examination, either step-scan or rapid-scan TR-SEIRA measurements were carried out. The photoconductive MCT detector equipped with a fast amplifier was used in the DC-coupled mode for the step-scan measurement. In the case of the rapid-scan measurements, the AC-coupled mode was utilized.

Step-scan measurements were carried out for the faster electron transfer processes when Cyt-c was electrostatically adsorbed on a C5- or C10-SAM. The time resolution was set to 100 μs covering the whole time-range for the redox reaction from 0 to 26 (250) ms for a single experiment in the case of C5-SAM (C10-SAM). The single-channel spectra were first measured at an applied electrode potential of −0.1 V for 5 (30) ms as a reference, then a potential jump to the redox potential at *ca.* +0.04 V for 7 (70) ms was carried out. Subsequently, the potential was set back to the initial value of −0.1 V for a relaxation time of 14 (150) ms. 1558 (200) coadditions were done to improve the signal-to-noise (S/N) ratio. Nine subsequently recorded sample single-channel spectra were averaged for the investigations with C10 to increase the S/N ratio further. An optical filter (< 1828 cm^{-1}) was used to reduce the number of the data points.

Measurements in the rapid scan mode were done when Cyt-c was adsorbed on C15-SAM. The time resolution was set to 500 ms and the experiment was repeated 256 times to increase the S/N ratio. In the same way as described before, single-channel spectra were measured with an applied electrode potential of −0.10 V (10 s) as reference, then the potential was set to the redox potential at *ca.* +0.04 V (20 s) and set back to the initial potential of −0.10 V (40 s).

Cyclic voltammetry

Cyclic voltammetric (CV) measurements were carried out with a potentiostat (multistat, CH Instruments, CH Labs-CHI 660b software), using two difference electrochemical cells, (i) the SEIRA set-up described above, and (ii) a set-up with home-made gold working electrodes fabricated from a gold wire (Good Fellow, 99.9%). The wire was heated under the hydrogen flame until the melted gold formed a ball which was polished with sand paper (3 M Technologies, Al_2O_3, different

grain size) and then boiled in concentrated nitric acid. The resulting plane surface exhibits an effective surface area of 2–4 mm^2. For CV measurements the surface was in contact with the bulk solution only *via* a meniscus. The Au working electrode of the SEIRA spectroelectrochemical cell was electrochemically cleaned by running CVs in 0.1 M H_2SO_4. After rinsing with water and ethanol, SAM formation was achieved as described above. For Cyt-c adsorption electrodes were immersed in Cyt-c solution with a Cyt-c concentration of 2 and 200 μM in case of the Au electrodes (i) and (ii) respectively. CV measurements of the immobilized protein were carried out in Cyt-c-free 30 mM phosphate buffer solution (I = 66 mM) at pH 7.0.

Results

Stationary SEIRA measurements

SEIRA spectroscopy is operated in the difference mode to enhance the sensitivity of the technique. To probe potential-dependent spectral changes difference spectra were constructed from SEIRA spectra measured at various electrode potentials using the SEIRA spectrum measured at −0.1 V as the reference. At this negative potential, the immobilised Cyt-c is in the reduced state such that SEIRA difference spectra obtained from measurements at more positive potentials reflect the redox-linked structural and orientational changes of the SAM/Cyt-c complex. Fig. 1 and 2 display such SEIRA difference spectra of Cyt-c immobilised on C15-SAM and on C10-SAM at different buffer concentrations corresponding to different ionic strengths. The most prominent difference signals are observed in the region of the amide I (1700–1620 cm^{-1}) and amide II modes (1540–1570 cm^{-1}) of the polypeptide backbone. Assignments for the amide I modes have been discussed by Ataka and Heberle.[6] Accordingly, the negative band at 1693-cm^{-1} has been assigned to a β-turn type III of the reduced Cyt-c whereas its counterpart in the oxidised form was attributed to the 1673-cm^{-1} band. Correspondingly, the 1666- and 1660-cm^{-1} bands were tentatively attributed to the amide I bands of a β-turn type II of reduced and oxidised Cyt-c, respectively, although the assignment to an α-helix segment cannot be ruled out.[6,13,14]

Comparison of the spectra measured at an ionic strength of 22 and 66 mM display different relative intensities particularly for Cyt-c immobilised on C15-SAM while the frequency remains unchanged. Taking the positive signals at *ca.* 1442 and 1420 cm^{-1} assigned by Susi and Byler[15] to CH_2 and CH_3 bending modes as a reference, the intensity of the 1693 cm^{-1} band decreases at higher ionic strength whereas the 1660-cm^{-1} band and, to a smaller extent, also the 1673-cm^{-1} band gain intensity. At an ionic strength of 22 mM the 1660-cm^{-1} band exhibits a higher intensity on C10-SAM as compared to C15-SAM, and it further increases with raising the ionic strength to 66 mM (see Fig. 2). At this ionic strength the intensity pattern of the 1673- and 1660-cm^{-1} bands is the same on C15-SAM where, however, a distinctly weaker signal at 1693 cm^{-1} is observed compared to C10-SAM.

On the first sight, the SEIRA difference spectra are quite different from the electrochemically induced IR difference

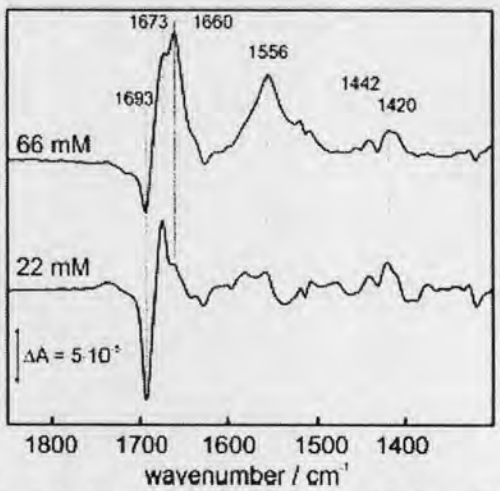

Fig. 1 SEIRA difference spectra of Cyt-c immobilised on a C15-SAM-coated Au electrode at different buffer concentrations. The spectra of the oxidized (positive bands) and reduced state (negative bands) were measured at +0.1 and −0.1 V, respectively.

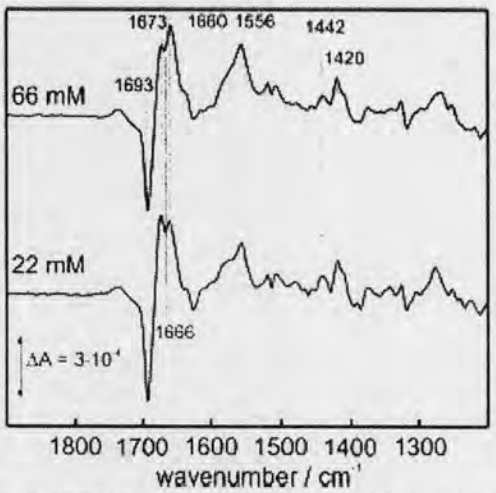

Fig. 2 SEIRA difference spectra of Cyt-c immobilised on a C10-SAM-coated Au electrode at different buffer concentrations. The spectra of the oxidized (positive bands) and reduced state (negative bands) were measured at +0.1 and −0.1 V, respectively.

spectrum of Cyt-c in solution (Fig. 3). A careful inspection, however, reveals that most of the positive and negative bands are present in both spectra albeit with different relative intensities. The most striking exception refers to the 1666- and 1660-cm^{-1} bands in the SEIRA difference spectrum since they are not observed in the IR difference spectrum of Cyt-c in solution which, in turn, displays a band pair at 1663 and 1651 cm^{-1}. It is tempting to assume that both band pairs originate from the same amide I modes, suggesting an adsorption-induced structural change of the underlying peptide

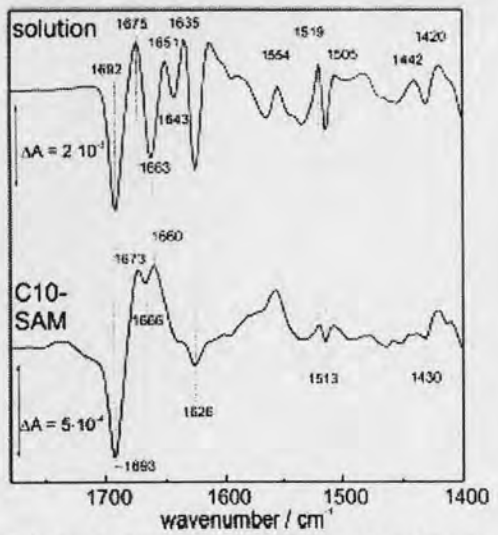

Fig. 3 SEIRA difference spectrum of Cyt-c on a C10-SAM-coated Au electrode (bottom) compared with the redox-induced IR difference spectrum of Cyt-c in solution (top). The positive and negative bands refer to the oxidized and reduced state, respectively. The respective spectra of the oxidised and reduced Cyt-c were obtained at +0.1 and −0.1 V, respectively. The SEIRA experiments were carried out at an ionic strength of 22 mM (pH 7.0).

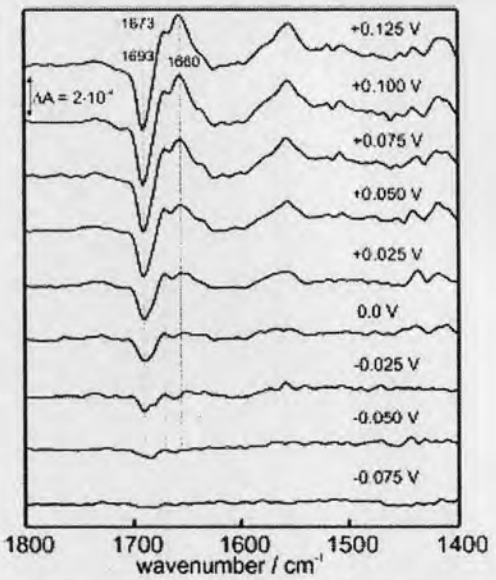

Fig. 4 SEIRA difference spectra of Cyt-c on a C10-SAM-coated Au electrode, obtained as a function of the potential. The positive and negative bands refer to the oxidized and reduced state, respectively. The reference spectrum of the reduced state was measured at −0.10 V. The experiments were carried out at an ionic strength of 66 mM (pH 7.0).

segments that leads to the frequency upshift in the reduced (+3 cm^{-1}) and oxidised form (+9 cm^{-1}). Moreover, this interpretation may support the assignment to an α-helix segment rather than to a β-turn type II.[13,14]

Measuring the SEIRA difference spectra as a function of the electrode potential allows determining the redox potential of the immobilised Cyt-c. Fig. 4 displays a selection of such spectra for which a spectrum measured at −0.1 v (fully reduced Cyt-c) was used as a reference. The intensities of the difference signals at 1673 and 1660 cm^{-1} (ferric Cyt-c) show a characteristic potential-dependence (Fig. 5) that can be described by the Nernst equation yielding a redox potential of 0.03 and 0.05 V, respectively, *i.e.*, a mean value of + 0.04 V. The number of transferred electrons derived from the fit is close to the theoretical value of one. The redox potential determined in this way was found to be the same for C15-, C10-, and C5-SAMs and independent of the ionic strength within the experimental accuracy (± 10 mV), as observed previously.[16,17] this value is only slightly more negative than the redox potential of Cyt-c in solution (between +0.05 and +0.06 V).[12,18]

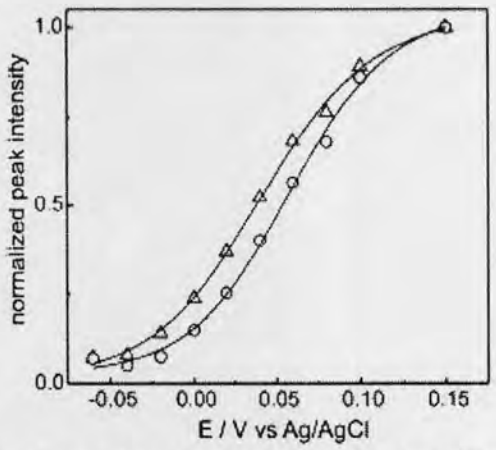

Fig. 5 Potential dependence of the peak height of the SEIRA difference bands at 1673 (triangles) and 1660 cm^{-1} (circles) as obtained from the potential-dependent SEIRA difference spectra. The solid line represents the fit of the Nernst equation to the experimental data.

Time-resolved SEIRA measurements

To probe the electron transfer dynamics of the immobilised Cyt-c, rapid potential jumps were applied to perturb the equilibrium at the initial potential E_{ref}. The subsequent relaxation processes that establish the equilibrium at the final potential E_f, were monitored by time-resolved SEIRA spectroscopy probing the temporal evolution of the bands at 1693 cm^{-1} (ferrous Cyt-c) and 1673 and 1660 cm^{-1} (ferric Cyt-c). We have chosen E_{ref} to be −0.1 V and E_f was set equal to the redox potential E^0 (+0.04 V).

For C15-SAMs the spectral changes were found to occur on the time scale of seconds which is appropriate to be probed by rapid-scan measurements (Fig. 6). For each band the

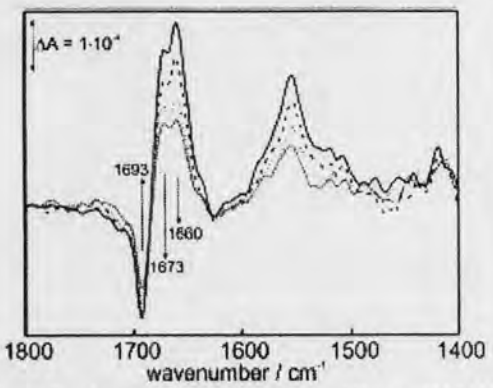

Fig. 6 Rapid-scan SEIRA difference spectra of Cyt-c on C15-SAM-coated Au electrodes using the spectrum measured at −0.1 V as a reference. The individual traces represent the difference spectra obtained at 1 (gray, dotted), 3 (gray, solid), 5 (black, dotted), 10 (black, dashed), and 20 (black, solid) s after the potential jump from −0.1 V to the redox potential (+0.04 V). The experiments were carried out at an ionic strength of 66 mM (pH 7.0).

time-dependent intensity changes can be well described by a mono-exponential kinetics with relaxation times τ that corresponds to a reciprocal relaxation constant $(k_{ret})^{-1}$ (Fig. 7). The analysis reveals a relaxation constant of *ca.* 0.40 and 0.20 s^{-1} for the 1693- and 1660-cm^{-1} band, respectively (Table 1). Whereas the kinetics derived from these bands is independent of the ionic strength, the relaxation constant describing the intensity changes of the 1673-cm^{-1} band decreases from 0.40 s^{-1} at low ionic strength to 0.20 s^{-1} at high ionic strength. This finding is consistent with the ionic-strength dependence of this band observed in the stationary SEIRA difference spectra (*vide supra*).

At C10-SAM, the spectral changes occur with much faster rates such that the step-scan technique is employed for the kinetic analysis (Fig. 8). In this case, similar relaxation rate constants (75–90 s^{-1}) are obtained for the 1693- and 1673-cm^{-1} bands, regardless of the ionic strength. Again a smaller value is obtained (*ca.* 50 s^{-1}) for the 1660-cm^{-1} band.

Whereas for both C15- and C10-SAMs, the error of the kinetic constants determined from the SEIRA experiments is estimated to be lower than 20%, step-scan measurements of Cyt-c on C5-SAM are associated with a larger uncertainty. Most likely, the lower stability and the higher structural heterogeneity of C5-SAMs are the main reasons for the substantially stronger scattering of the kinetic constants in the individual measurements. Thus, the error is estimated to be two times larger than for C10- and C15-SAMs, *i.e.*, *ca.* 40%. However, the results unambiguously indicate a further acceleration of the relaxation processes. The average relaxation constants that are derived from the intensity changes of the 1693-, 1673-, and 1660-cm^{-1} bands are determined to be of 900, 700, and 600 s^{-1}. Within the experimental error, these values were found to be the same at an ionic strength of 66 and 130 mM. Note that at these ionic strengths the response time of the SEIRA electrochemical cell was better than 400 μs.

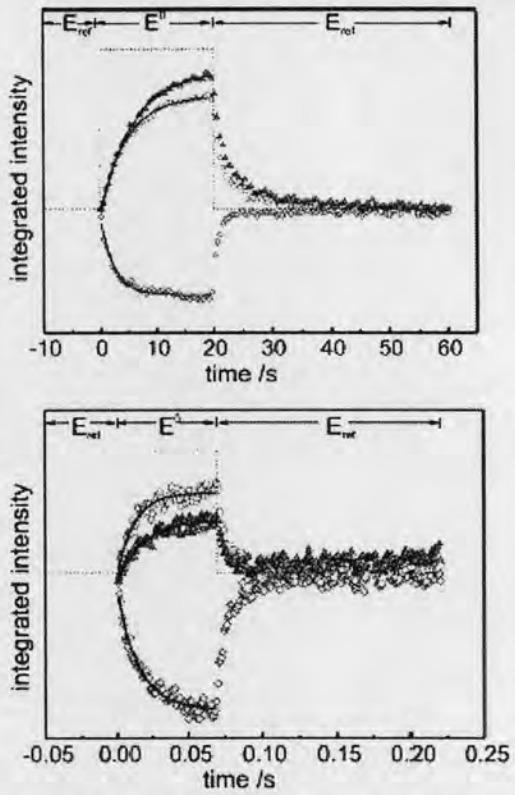

Fig. 7 Kinetic traces of the time-evolution of the SEIRA bands at 1693 cm^{-1} (gray squares; reduced), 1673 cm^{-1} (white circles, oxidised), and 1660 cm^{-1} (dark gray triangles, oxidised) obtained from the rapid scan and step scan SEIRA spectroscopic measurements of Cyt-c on C15-SAM (top) and C10-SAM (bottom), respectively (see Fig. 6 and 8).

Cyclic voltammetry

CV measurements were carried out with the SEIRA electrode and, alternatively, with a gold wire electrode, which possess a surface area of 2.52 cm^2 *vs.* 2–4 mm^2, respectively. Regardless of the different surface areas, the same standard electron transfer rate constants were obtained with both devices. Fig. 9 shows typical CVs for the immobilised Cyt-c on C10- and C15-SAM coated electrodes. The CVs present clear redox peaks with small peak-to-peak separations ΔE_p for C10- and C5-SAMs. The voltammograms are nearly reversible with ΔE_p < 0.040 V for CV scan rates up to 0.4 and 1.5 V s^{-1} in the case for C10-SAM and C5-SAMs, respectively. Within these ranges of the scan rates, the full-width at half height is 0.09–0.12 V. Up to a scan rate of 8.0 V s^{-1} for C10-SAMs and 20 V s^{-1} for C5-SAMs, the peak separation is still less than 0.20 V. Because of the small electron transfer rate constant for C15-SAM, the voltammograms display deviations from the shape expected for a reversible behaviour since the peaks are broadened and ΔE_p is already larger than 0.2 V at a scan rate 0.05 V s^{-1}. The average redox potentials of the immobilised Cyt-c measured at

Table 1 Relaxation constants for the potential jump from −0.1 V to the redox potential for Cyt-c immobilised on coated electrodes as determined by rapid scan and step scan SEIRA spectroscopy[a,b]

System/technique			C15-SAM	C10-SAM	C5-SAM
SEIRA, Au	1693 cm^{-1} (red.)	$k_{\text{prot,relax}}$	0.4 s^{-1}	75 s^{-1}	900 s^{-1}
		$k_{\text{prot}}^{\text{red}}$	0.2 s^{-1}	38 s^{-1}	450 s^{-1}
	1673 cm^{-1} (ox.)	$k_{\text{prot,relax}}$	0.2 s^{-1} (0.4 s^{-1})	90 s^{-1}	700 s^{-1}
		$k_{\text{prot}}^{\text{ox}}$	0.1 s^{-1} (0.2 s^{-1})	45 s^{-1}	350 s^{-1}
	1660 cm^{-1} (ox.)	$k_{\text{prot,relax}}$	0.2 s^{-1}	50 s^{-1}	600 s^{-1}
		$k_{\text{prot}}^{\text{ox}}$	0.1 s^{-1}	25 s^{-1}	300 s^{-1}
CV, Au		k_{ET}	0.14 s^{-1}	40 s^{-1}	245 s^{-1}[d]
SERR, Ag[c]	Heme modes	$k_{\text{redox,heme}}$	0.15 s^{-1}	85 s^{-1}	270 s^{-1}
		k_{ET}	0.08 s^{-1}	43 s^{-1}	
	Heme modes	k_{rel}	>6000 s^{-1}	380 s^{-1}	250 s^{-1}

[a] Kinetic data refer to pH 7.0 at ionic strength of 66 mM. The rate constants are defined by eqns (2) and (3) and in Fig. 11. [b] Relaxation constant determined for an ionic strength of 22 mM (pH 7.0). [c] Taken from ref. 11 and 28. [d] Apparent rate constant reflecting a process other than electron tunneling.

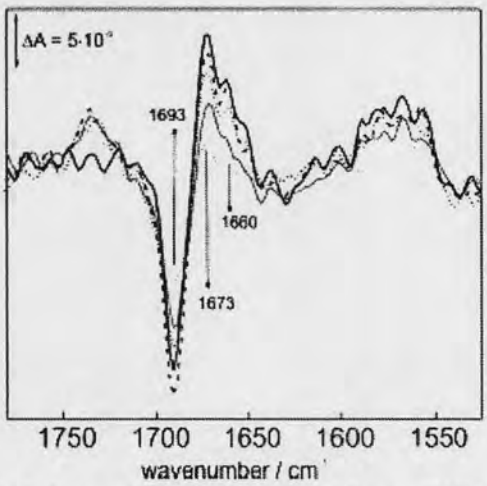

Fig. 8 Step-scan SEIRA difference spectra of Cyt-c on C10-SAM coated Au electrodes using the spectrum measured at −0.1 V as a reference. The individual traces represent the difference spectra obtained at 5 (gray, dotted), 10 (gray, solid), 20 (black, dotted), 40 (black, dashed), and 70 (black, solid) ms after the potential jump from −0.1 V to the redox potential (+0.04 V). The experiments were carried out at an ionic strength of 66 mM (pH 7.0).

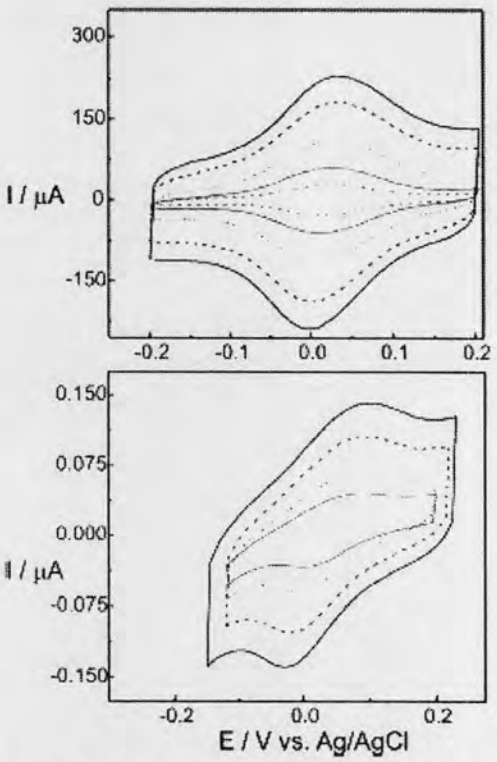

Fig. 9 CVs of immobilised Cyt-c on C10-SAM (top) at scan rates of 0.05, 0.1, 0.2, 0.4, 0.8 and 1.0 V s^{-1}; and on C15-SAM (bottom) at scan rates of 1, 2, 4, 7.5 and 10 mV s^{-1}. The experiments were carried out at an ionic strength of 66 mM (pH 7.0) using the SEIRA electrochemical cell.

an ionic strength of 66 mM (pH 7.0) are 0.036 V which are slightly negatively shifted from that of Cyt-c in solution (0.05–0.06 V).

As shown in Fig. 10, the peak current increases linearly with the scan rate, indicating a surface-confined electrode process of the immobilized Cyt-c. Employing Laviron's method, the corresponding standard electron transfer rate constants k_{ET} can be deduced from the peak separation of the voltammogram *vs.* the scan rate.[19] For ΔE_p < 0.2 V, one obtains a value of 0.14, 40, and 250 s^{-1} for C15-, C10-, and C5-SAMs (Table 1).

The surface roughness factor (R_f) of the active SEIRA surface was electrochemically determined to be 2.8 by measuring the gold oxide reduction charge density.[20] The value is similar to that found by Miyake (R_f = 2.5) obtained with the same preparation for the SEIRA active surface.[9]

According to

$$I_p = n^2F^2\nu A\Gamma/4RT \quad (1)$$

where I_p, A and ν represent the average peak current, effective electrode surface and scan rate, respectively, an average surface coverage Γ of the immobilized Cyt-c is estimated to be 8, 9

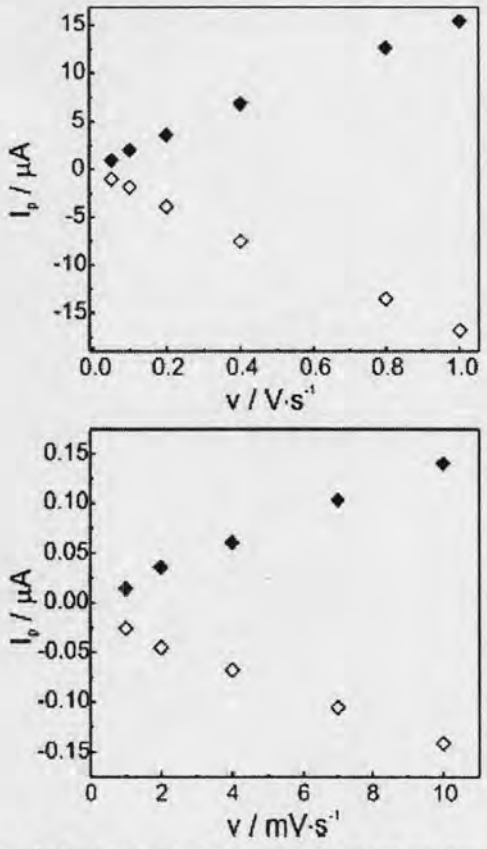

Fig. 10 Relationship between peak current and scan rate derived from the CVs of immobilised Cyt-c on C10-SAM (top) and on C15-SAM (bottom). Anodic and cathodic currents are given by close and open symbols, respectively. The experiments were carried out at an ionic strength of 66 mM (pH 7.0) using the SEIRA electrochemical cell.

and 10 pmol cm^{-2} for C15-, C10- and C5-SAMs, respectively. These values are somewhat lower than the theoretical maximum coverage of 15 pmol cm^{-2}.[16]

Discussion

Structural changes probed by SEIRA spectroscopy

The SEIRA difference bands that are found to be linked with the interfacial redox process of Cyt-c have also been observed in a previous SEIRA study by Ataka and Heberle.[6] These authors assigned the 1693 and 1673 cm^{-1} bands to the β-turn III segments 14–19 or 67–70 of the reduced and oxidised form, respectively. The assignment of the 1660- and 1666-cm^{-1} bands to specific peptide segments is less clear.[13,14] In principle, SEIRA difference signals may result from structural or orientational changes of the peptide segments,[2] either induced by the variation of the electrode potential or the redox state change of the heme.

Let us first consider the 1693- and 1673-cm^{-1} band pair which exhibits the same frequencies as in the redox-linked difference spectrum in solution. Thus, in this case, direct effects of the electrode potential that are redox-state independent can be ruled out and this band pair evidently reflects the same redox-linked structural changes of the β-turn III segment in the adsorbed state as in solution. These changes are likely to be very small and clearly beyond the level of secondary structure changes as in both cases the difference signals exhibit only 1–2% absorbance of the absolute band intensity suggesting the involvement of only one or two peptide bonds. In fact, Berghuis and Brayer[21] have demonstrated that redox-linked conformational changes of crystalline yeast iso-1 Cyt-c are restricted to small adjustments of the heme geometry, rearrangements of internal water molecules, and changes of thermal parameters of individual peptide segments. Among the latter are the residues 65–72, specifically Tyr67, which is consistent with the assignment of the 1693/1673-cm^{-1} band pair to the β-turn III segment 67–70. The situation is different for the 1666/1660-cm^{-1} band pair which is shifted to higher frequencies as compared to the solution spectrum. These findings point to a structural change of the underlying peptide segment brought about by immobilisation.

The SEIRA intensities of the amide I bands depend on the orientation of the peptide bonds with respect to the surface. If the intensity ratio of the conjugate peaks is similar as in solution, the redox transition will not be associated with an orientational change of the peptide segments involved. This appears to be the case for Cyt-c adsorbed on C15-SAM at low ionic strength and on C10-SAM independent of the ionic strength. For Cyt-c on C15-SAM at high ionic strength, however, the drastic decrease of the 1693-cm^{-1} peak height and the increase of the 1673-cm^{-1} band intensity suggest a redox-state-dependent orientational change of β-turn III segment 67–70. Concomitantly, the intensity of the 1660-cm^{-1} considerably increases on C15-SAM and, to a minor extent, also on C10-SAM upon raising the ionic strength, implying a reorientation of the underlying peptide segment in the oxidised state. These variations of the amide band intensities most likely have a common origin: both the thickness of the SAM, *i.e.*, the separation of Cyt-c from the electrode, and the ionic strength are parameters that control the electric field strength at the protein binding site,[3,4,10] which in turn is likely to affect the orientation of individual peptide segments. Such orientational changes may either result from the alteration of the tertiary structure or from the reorientation of the entire immobilised protein (*vide infra*).

Electron transfer dynamics

Previous studies on Cyt-c immobilised on SAM-coated electrodes have revealed an unusual distance dependence of the electron transfer kinetics.[11,22–24] Whereas at SAMs with chain lengths longer than C10 the kinetics can be ascribed to an electron tunnelling mechanism, SAMs with shorter SAM lengths (<C10) show distance-independent rate constants implying that a process other than electron tunnelling is rate-limiting.[3,4,11,24–27] This phenomenon has been observed by various techniques and different electrochemical systems

and proteins. In a recent SERR spectroscopic study on SAM-coated Ag electrodes we have shown that this rate-limiting step is the re-orientation of the entire immobilised Cyt-c.[28] Since the orientation of the heme with respect to the SAM surface is a crucial parameter controlling the electron tunnelling rate, the rate of the overall redox process is modulated by the rate of re-orientation, which may be imagined as a rotational diffusion. This process, however, sensitively depends on the local electric field and thus its rate constant decreases from long to short SAM lengths, whereas for a given orientation the electron tunnelling rate increases exponentially with decreasing distance to the electrode.

For C-15-SAM, the reorientation rate constant (k_{rot}) has been found to be larger than 6000 s^{-1} whereas for the redox transition a relaxation constant k_{redox} of 0.15 s^{-1} has been determined.[11,28] Since these SERR experiments—like the present SEIRA measurements—were carried out with potential jumps to the redox potential, the forward and backward electron transfer reactions (k_{ET}^{ox}, k_{ET}^{red}) are both associated with a driving force of 0 eV, *i.e.*

$$k_{redox} = k_{ET}^{ox} + k_{ET}^{red} = 2k_{ET} \qquad (2)$$

such that the formal heterogeneous electron transfer rate constant k_{ET} is *ca.* 0.08 s^{-1}.

Unlike the SERR measurements that directly probe the redox state change of the heme, the kinetic constants derived from the SEIRA experiments refer to the temporal evolution of band intensities of the protein matrix (k_{prot}^{ox}, k_{prot}^{red}). These amide I band changes reflect structural and orientational changes of individual peptide segments that are induced by the redox state change of the heme and may occur with the same rate as electron tunneling, or may follow the electron transfer step. Thus, in the simplest case, one may describe the processes of Cyt-c that are induced by the potential jump to the redox potential by the scheme sketched in Fig. 11. For the potential jump from −0.1 V to the redox potential, SEIRA experiments monitor the oxidation of the immobilised Cyt-c (bold arrows in Fig. 11). Electron transfer preferentially occurs *via* an orientation of the immobilised protein that provides the optimum electronic coupling for electron tunnelling. This is easily achieved for the C15-SAM since re-orientation of the oxidised and reduced Cyt-c on the SAM surface is much faster (> 6000 s^{-1}; *vide supra*) than electron tunnelling (0.08 s^{-1}).[28] These rate constants have been determined for Cyt-c on SAM-coated Ag electrodes and may differ somewhat in the case of Au electrodes (*vide supra*). However, it is very likely that also for Au/C15-SAM and Au/C10-SAM systems protein rotation is distinctly faster than electron tunneling, *i.e.*, $k_{rot} \gg k_{ET}$. In fact, this conclusion is supported by the present and previous CV measurements that afford an electron transfer rate constant of *ca.* 0.14 s^{-1} which is somewhat larger than that for the Cyt-c/C15-SAM/Ag system.[11,22–24] Correspondingly, the rate of the potential-dependent re-orientation of the entire protein is expected to be of the same order of magnitude for C15-SAM coated Ag and Au electrodes such that the relatively slow rates for the amide I band changes are attributed to secondary and tertiary structure changes which may involve a re-orientation of an individual peptide segment rather than a "rotation" of the protein. Accordingly, adaptation of the protein to the new electron density distribution of the heme and the dipole moment change of Cyt[29] that is brought about by the electron transfer step follows in two steps, (i) fast re-orientation of the entire protein on the SAM surface and (ii) much slower subtle changes of the secondary and tertiary structure. At low ionic strength, these structural changes take place with a relaxation constant of 0.4 s^{-1} for the band pair at 1693 and 1673 cm^{-1} and 0.2 s^{-1} for the 1660-cm^{-1} band. In a first approximation one may relate these relaxation constants k_{prot} to the rate constants of the protein structural changes upon oxidation and reduction (k_{prot}^{ox}, k_{prot}^{red}) in analogy to eqn (2)

$$k_{prot,relax} = k_{prot}^{ox} + k_{prot}^{red} = 2k_{prot} \qquad (3)$$

implying that the structural changes of the β-turn III segment 67–70 occur with 0.2 s^{-1} (k_{prot}) and thus take place with about the same rate as the electron transfer ($k_{ET} \cong 0.14$ s^{-1}). The structural changes related to the 1660-cm^{-1} band proceed with a two times slower rate. At high ionic strength (66 mM), the structural changes reflected by the 1673-cm^{-1} band are slowed down by a factor of two whereas all other rate constants remain unchanged.

On C10-SAMs the same reaction mechanism holds. However, the rate constants of the individual reaction steps are different. The electron transfer rate constant increases to 40 s^{-1} as determined by the CV measurements. This value is in very good agreement with the rate constant obtained for Cyt-c on C10-SAM-coated Ag electrodes by SERR spectroscopy (43 s^{-1}). Conversely, the re-orientation rate constant for the C10-SAM/Ag system decreases to 380 s^{-1} which is, however, still much faster than electron tunneling and the protein structural changes monitored by SEIRA spectroscopy. The latter processes take place with the same rate constant (*ca.* 42 s^{-1}) as electron tunnelling in the case of the β-turn III structural changes and are, as for C15-SAM, somewhat slower (25 s^{-1}) for the changes of the amide I band at 1660 cm^{-1}.

The kinetics of the interfacial redox process is further accelerated at the C5-SAM but is by far too slow to be attributed to electron tunnelling as the rate-limiting step. The average values for the kinetic constants obtained from the temporal evolution of the three SEIRA difference bands may follow a similar pattern as for C10- and C15-SAM, *i.e.* that the time-dependence of the 1660-cm^{-1} bands is slower than those of the 1693- and 1673-cm^{-1} bands. However, the experimental uncertainty associated with the measurements of the C5-SAMs does not allow an unambiguous confirmation of this conclusion. Moreover, also the error margin of CV data is likely to be distinctly higher. The apparent electron transfer constant determined in this work (*ca.* 245 s^{-1}) is at the lower limit of the values obtained by previous CV or electroreflectance measurements (450 to 1000 s^{-1}).[22,23] Taking into account the considerable scattering of these data we conclude that, within the experimental accuracy, protein relaxation processes and electron transfer occur with very similar rates.

For Cyt-c Ag/C5-SAM, protein rotation has been identified as the rate-limiting step of the interfacial redox process since

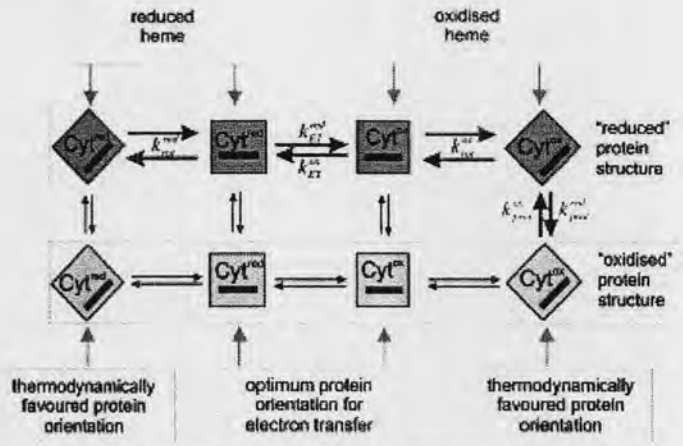

Fig. 11 Model for the reaction mechanism of the interfacial redox process of Cyt-c immobilised on SAM-coated electrodes. The reaction pathway studied in this work is highlighted by the bold arrows. k_{rot}^{ox} and k_{rot}^{red} refer to the relaxation constants for rotational diffusion, monitored by TR SERR spectroscopy, whereas k_{prot}^{ox} and k_{prot}^{red}, derived from SEIRA measurements, denote the rate constants of the protein structural changes to adapt the equilibrium structure of the reduced and oxidised Cyt-c, respectively. k_{ET}^{ox} and k_{ET}^{red} are the standard heterogeneous electron transfer rate constants at zero driving force (see eqn (2)).

the apparent ET constant is equal to the protein rotational relaxation (Table 1). There is no indication that this is not the case for the Au/C5-SAM system. However, since k_{rot} could not be determined directly on Au/C5-SAM, we cannot ultimately exclude protein structural changes as probed by the step-scan SEIRA measurements to be rate-limiting. Conversely, it may be that the intensities of amide I band difference signals are modulated by the protein rotation due to the orientation-dependent surface enhancement in the IR absorption.

Electric field effects on the interfacial redox process

The present results of the distance dependence of the electron transfer dynamics and those previously obtained by TR SERR spectroscopy on Ag/SAM[11] and by electrochemistry on Au/SAM electrodes,[22,23] are consistent with the view that at SAM lengths shorter than C10 the overall rate of the electron transfer process is limited by a reaction step other than electron tunneling and eventually becomes distance-independent. Differences are noted for the values of the rate constants for the rate-limiting step which for Au/C5-SAM (SEIRA, CV) is larger by *ca.* a factor of 2 than for Ag/C5-SAM (SERR) (Table 1; ref. 23). This discrepancy is attributed to the effect of the electric field in the SAM/protein interface. For the Ag/SAM system this parameter has been shown to slow down the re-orientation of the immobilised protein (rotational diffusion) such that it becomes the rate limiting step at Ag/C5-SAM with $k_{rot} = 250\ s^{-1}$. We therefore assume that the electric field is weaker in the SAM/protein interface on Au compared to Ag electrodes.

The electric field strength at the protein/SAM interface can be described on the basis of a simple electrostatic model originally proposed by Smith and White[10] and later adapted to the electrode/SAM interface.[10] Accordingly, the electric field strength E_{EF} may be approximated by

$$E_{EF} = \frac{-\sigma_C d_{RC} + \varepsilon_0 \varepsilon_P (E - E_{pzc})}{\varepsilon_0 (d_C \varepsilon_P + d_{RC} \varepsilon_C)} \qquad (4)$$

where σ_C is the charge densities on the SAM surface and at the redox center, respectively (see ESI).† The quantities d_C, d_{RC}, ε_P, and ε_C refer to the thickness of the SAM, the distance between the SAM and the redox center, the dielectric constant in the protein and in the SAM, respectively. E and E_{pzc} are the electrode potential and the potential of zero charge, and ε_0 is the permittivity. Eqn (4) indicates that E_{EF} mainly depends on three parameters. It increases with decreasing distance to the electrode (d_C) and increasing charge density in the protein/SAM interface (σ_C). These two parameters may be similar albeit not identical for both the Au and the Ag electrode. The third parameter is the potential of zero charge E_{pzc} which is >0.0 and *ca.* −0.7 V for Au and Ag, respectively.[31–34] Thus, for electrode potentials around the redox potential of Cyt, $(E - E_{pzc})$ is negative for Ag but positive or close to zero for Au. Since σ_C is negative, the electric field strength is larger for Ag than for Au. This conclusion is consistent with the fact that the potential-drop across the Au/SAM/Cyt-c interface which is reflected by a shift in the redox potential is much smaller than for the Ag system. Correspondingly, one may readily rationalise the two-times slower kinetics of the rate-limiting step (*i.e.*, protein rotation) on Ag/C5-SAM in terms the higher electric field strength, as compared to the Au/C5-SAM.

For longer chain lengths, electron tunneling is the rate-limiting step on both the Ag/SAM and Au/SAM systems. The values obtained for the electron transfer rate constant obtained by CV (Au) and SERR (Ag) are the same for both metals for the C10-SAM, whereas for the C15-SAM somewhat

larger rate constants are determined for the Au/C15-SAM system. This discrepancy may be due to a slightly different structural organisation of the SAMs on Au and Ag that may include different tilt angles of the aliphatic chains with respect to the surface.[35–38] This may have consequences for the tunneling distances for longer chain lengths (C15-SAM) and thus affect the electron transfer rate constant. Note that just a decrease of the tunneling distance by 0.5 Å can readily account for the different rate constants determined for Au/C15-SAM and Ag/C15-SAM.

We cannot exclude that the electric field affects the dynamics of the protein structural changes as monitored by SEIRA spectroscopy. However, the present data are consistent with the view that, regardless of the chain length and thus independent of the electric field, the protein structural changes follow the electron transfer. Thus, the simplified reaction model depicted in Fig. 11 may represent a reasonable approximate description for the interfacial redox processes of Cyt-c in general.

Conclusions

1. SEIRA spectroscopy of immobilised Cyt-c allows detecting redox-linked protein structural changes. The conjugate difference bands at 1693 and 1673 cm^{-1}, tentatively assigned to the β-turn type III segment 67–70, have also been observed in redox-induced difference spectra of Cyt-c in solution whereas the SEIRA signal at 1660-cm^{-1} is characteristic of the immobilised protein and may reflect subtle redox-dependent structural *and* orientational changes of one or more amide bonds.

2. The redox potentials determined by CV and stationary SEIRA spectroscopy do not differ significantly from that in solution and do not display a distance-dependence.

3. The electron transfer rate constant at C15-SAMs, determined by CV on Au, is slightly larger than that on Ag electrodes obtained by SERR spectroscopy,[11,22–24] which may be attributed to different SAM structures. For C10-SAMs the electron tunnelling rate constant is the same for both metals.

4. The β-turn type III structural changes (1693/1673 cm^{-1}) occur with the same time-dependence as the electron transfer step whereas the amide bond changes revealed by the 1660-cm^{-1} band proceed with a somewhat slower kinetics, at least for C10- and C15-SAMs.

5. It is very likely that, in analogy to previous findings for SAM-coated Ag electodes,[23] rotational diffusion of Cyt-c represents the rate-limiting step of the interfacial redox process at SAM-coated Au-electrodes for SAM lengths shorter than C10. There is no indication that the protein structural (and orientational) changes reflected by the SEIRA difference bands depend on the local electric field strength at the SAM/protein interface.

6. In the distance-independent regime of the interfacial redox process, the rate constant for the limiting step is distinctly larger for Au than for Ag which is attributed to different electric field strengths.

7. Rapid scan and step scan SEIRA spectroscopy provide novel insight into redox-linked protein dynamics and mechanistic details of interfacial processes, thereby complementing the information obtained by electrochemical methods and TR SERR spectroscopy.

Acknowledgements

The authors wish to thank Diego Millo and Dr Jiu-Ju Feng for critical comments. The support by Drs Ken Ataka and Joachim Heberle in establishing the SEIRA technique in our laboratory is gratefully acknowledged. The work was supported by the DFG (Sfb 498, Cluster of Excellence "Unifying concepts in catalysis"), the Volkswagen-Foundation (I/80816), and ANPCyT (PICT2006-459). NW was supported by the DAAD-TRF/RGJ scholarship and a fellowship from the Thailand Research Fund *via* the Royal Golden Jubilee PhD Program (PHD/0107/2545) to SE.

References

1 *Bioelectronics—From Theory to Applications*, ed. I. Willner and E. Katz, Wiley-VCH, Weinheim, 1st edn, 2005.
2 F. Siebert and P. Hildebrandt, *Vibrational Spectroscopy in Life Science*, Wiley-VCH, Weinheim, 1st edn, 2008.
3 D. H. Murgida and P. Hildebrandt, *Phys. Chem. Chem. Phys.*, 2005, 7, 3773.
4 D. H. Murgida and P. Hildebrandt, *Chem. Soc. Rev.*, 2008, 37 937.
5 G. Smulevich and T. G. Spiro, *J. Phys. Chem.*, 1985, 89, 5168.
6 K. Ataka and J. Heberle, *J. Am. Chem. Soc.*, 2004, 126, 9445.
7 K. Ataka, F. Giess, W. Knoll, R. Naumann, S. Haber-Pohlmeier, B. Richter and J. Heberle, *J. Am. Chem. Soc.*, 2004, 126 16199.
8 K. Ataka and J. Heberle, *Anal. Bioanal. Chem.*, 2007, 388, 47.
9 H. Miyake, S. Ye and M. Osawa, *Electrochem. Commun.*, 2002, 4, 973.
10 D. H. Murgida and P. Hildebrandt, *J. Phys. Chem. B*, 2001, 105, 1578.
11 D. H. Murgida and P. Hildebrandt, *J. Am. Chem. Soc.*, 2001, 123, 4062.
12 D. Moss, E. Nabedryk, J. Breton and W. Mantele, *Eur. J. Biochem.*, 1990, 187, 565.
13 D. D. Schlereth and W. Mantele, *Biochemistry*, 1992, 31, 7494.
14 A. Dong, P. Huang and W. S. Caughey, *Biochemistry*, 1992, 31, 182.
15 H. Susi and D. M. Byler, *Biochem. Biophys. Res. Commun.*, 1983, 115, 391.
16 S. Song, R. A. Clark, E. F. Bowden and M. J. Tarlov, *J. Phys. Chem.*, 1993, 97, 6564.
17 R. A. Clark and E. F. Bowden, *Langmuir*, 1997, 13, 559.
18 M. J. Eddowes and H. A. O. Hill, *J. Am. Chem. Soc.*, 1979, 101, 4461.
19 E. Laviron, *J. Electroanal. Chem.*, 1979, 101, 19.
20 M. C. Leopold, J. A. Black and E. F. Bowden, *Langmuir*, 2002, 18, 978.
21 A. M. Berghuis and G. D. Brayer, *J. Mol. Biol.*, 1992, 223, 959.
22 Z. Q. Feng, S. Imabayashi, T. Kakiuchi and K. Niki, *J. Chem. Soc., Faraday Trans.*, 1997, 93, 1367.
23 M. T. de Groot, M. Merkx and M. T. M. Koper, *Langmuir*, 2007, 23, 3832.
24 A. Avila, B. W. Gregory, K. Niki and T. M. Cotton, *J. Phys. Chem. B*, 2000, 104, 2759.
25 H. J. Yue, D. Khoshtariya, D. H. Waldeck, J. Grochol, P. Hildebrandt and D. H. Murgida, *J. Phys. Chem. B*, 2006, 110, 19906.
26 J. J. Wei, H. Y. Liu, A. R. Dick, H. Yamamoto, Y. F. He and D. H. Waldeck, *J. Am. Chem. Soc.*, 2002, 124, 9591.
27 T. D. Dolidze, S. Rondinini, A. Vertova, D. H. Waldeck and D. E. Khoshtariya, *Biopolymers*, 2007, 87, 68.
28 A. Krnjetic, K. H. Ly, P. Hildebrandt and D. H. Murgida, *J. Am. Chem. Soc.*, 2008, in press.

29 W. H. Koppenol, J. D. Rush, J. D. Mills and E. Margoliash, *Mol. Biol. Evol.*, 1991, 8, 545.
30 C. P. Smith and H. S. White, *Anal. Chem.*, 1992, 64, 2398.
31 G. Valette and A. Hamelin, *J. Electroanal. Chem.*, 1973, 45, 301.
32 A. V. Shlepakov and E. S. Sevastyanov, *Sov. Electrochem.*, 1978, 14, 243.
33 P. Ramirez, R. Andreu, A. Cuesta, C. J. Calzado and J. J. Calvente, *Anal. Chem.*, 2007, 79, 6473.
34 A. Hamelin, *J. Electroanal. Chem.*, 1983, 144, 365.
35 M. M. Walczak, C. K. Chung, S. M. Stole, C. A. Widrig and M. D. Porter, *J. Am. Chem. Soc.*, 1991, 113, 2370.
36 J. C. Love, L. A. Estroff, J. K. Kriebel, R. G. Nuzzo and G. M. Whitesides, *Chem. Rev.*, 2005, 105, 1103.
37 P. E. Laibinis, G. M. Whitesides, D. L. Allara, Y. T. Tao, A. N. Parikh and R. G. Nuzzo, *J. Am. Chem. Soc.*, 1991, 113 7152.
38 C. D. Bain, E. B. Troughton, Y. T. Tao, J. Evall, G. M. Whitesides and R. G. Nuzzo, *J. Am. Chem. Soc.*, 1989, 111, 321.

CURRICULUM VITAE

Date of Birth: April 8, 1978 **Birth Place:** Mukdaharn, Thailand

Address: 5 Chayangkool Kho Road, Tumbol Mukdaharn, Amphur Muang, Mukdaharn 49000, Thailand

Education:

Ph.D. / Chemistry	2008	Chulalongkorn University/Thailand
B.Sc. (hons) / Chemistry	1999	Ubon Ratchathani University/Thailand

Research Publications:

1. **Wisitruangsakul, N.;** Zebger, I.; Ly, H. K.; Murgida, H. D.; Ekgasit, S.; and Hildebrandt, P. Redox-Linked Protein Dynamics of Cytochrome c Probed by Time-Resolved Surface Enhanced Infrared Absorption Spectroscopy. Physical Chemistry Chemical Physics 10 (2008): 5276–5286.
2. Todorovic, S.; Verissimo, A.; **Wisitruangsakul, N.;** Zebger, I.; Hildebrandt, P.; Pereira, M. M.; Teixeira, M.; and Murgida, D. H. The Journal of Physical Chemistry B 112 (2008): 16952–16959.
3. **Wisitruangsakul, N.;** Lenz, O.; Ludwig, M.; Friedrich, B.; Lendzian, F.; Hildebrandt, P.; and Zebger, I. Monitoring catalysis of the membrane-bound hydrogenase from Ralstonia eutropha H16 by surface-enhanced IR absorption spectroscopy. Angewandte Chemie International Edition 48 (2009): 611-613.
4. Ludwig, M.; Schubert, T.; Zebger, I.; **Wisitruangsakul, N.;** Saggu M.; Strack A.; Lenz, O.; Hildebrandt, P.; and Friedrich, B. Concerted action of two novel auxiliary proteins in assembly of the active site in a membrane-bound [NiFe] hydrogenase. The Journal of biological chemistry 284 (2009): 2159-2168.
5. **Wisitruangsakul, N.;** Lenz, O.; Ludwig, M.; Friedrich, B.; Lendzian, F.; Hildebrandt, P.; and Zebger, I. Untersuchung des Katalyseprozesses der membrangebundenen Hydrogenase aus Ralstonia eutropha H16 mittels oberflächenverstärkter IR-Absorptionsspektroskopie Angewandte Chemie 121 (2009): 621-623.

Scholarship and Awards:

2002-2008	:	The Royal Golden Jubilee (RGJ) Ph.D. Scholarship supported by Thailand Research Fund/Thailand
2004-2005	:	DAAD-RGJ Scholarship/Germany
2006-2008	:	Volkswagen-Foundation (I/80816)/Germany
2008	:	DFG, Cluster of Excellence "Unifying Concepts in Catalysis"/Germany
2008	:	Outstanding Oral Presentation Award/ the Pure and Applied Chemistry International Conference 2009